



This is a repository copy of *Anomalous dielectric behaviour at the monoclinic to tetragonal phase transition in La(Nb<sub>0.9</sub>V<sub>0.1</sub>)O<sub>4</sub>*.

White Rose Research Online URL for this paper:  
<https://eprints.whiterose.ac.uk/167673/>

Version: Accepted Version

---

**Article:**

Zhou, D., Guo, H.-H., Fu, M.S. et al. (8 more authors) (2021) Anomalous dielectric behaviour at the monoclinic to tetragonal phase transition in La(Nb<sub>0.9</sub>V<sub>0.1</sub>)O<sub>4</sub>. *Inorganic Chemistry Frontiers*, 8 (1). pp. 156-163. ISSN 2052-1553

<https://doi.org/10.1039/d0qi00981d>

---

© 2020 Royal Society of Chemistry. This is an author-produced version of a paper subsequently published in *Inorganic Chemistry Frontiers*. Uploaded in accordance with the publisher's self-archiving policy.

**Reuse**

Items deposited in White Rose Research Online are protected by copyright, with all rights reserved unless indicated otherwise. They may be downloaded and/or printed for private study, or other acts as permitted by national copyright laws. The publisher or other rights holders may allow further reproduction and re-use of the full text version. This is indicated by the licence information on the White Rose Research Online record for the item.

**Takedown**

If you consider content in White Rose Research Online to be in breach of UK law, please notify us by emailing [eprints@whiterose.ac.uk](mailto:eprints@whiterose.ac.uk) including the URL of the record and the reason for the withdrawal request.



[eprints@whiterose.ac.uk](mailto:eprints@whiterose.ac.uk)  
<https://eprints.whiterose.ac.uk/>

## ARTICLE

## Anomalous Dielectric Behaviour at the Monoclinic to Tetragonal Phase Transition in $\text{La}(\text{Nb}_{0.9}\text{V}_{0.1})\text{O}_4$

Received 00th January 20xx,  
Accepted 00th January 20xx

DOI: 10.1039/x0xx00000x

Di Zhou,<sup>\*a</sup> Huan-Huan Guo,<sup>a</sup> Mao-Sen Fu,<sup>b</sup> Xiao-Gang Yao,<sup>c</sup> Hui-Xing Lin,<sup>c</sup> Wen-Feng Liu,<sup>d</sup> Li-Xia Pang,<sup>f</sup> Charanjeet Singh,<sup>g</sup> Sergei Trukhanov<sup>h,i,j</sup> and Alex Trukhanov<sup>h,i,j</sup> & Ian M. Reaney<sup>\*e</sup>

$\text{La}(\text{Nb}_{0.9}\text{V}_{0.1})\text{O}_4$  has been shown by *in-situ* Raman spectra and X-ray diffraction to undergo a ferroelastic phase transition from monoclinic fergusonite to tetragonal scheelite ( $T_{M-T}$ ) at 350 °C, accompanied by 3.55% spontaneous strain and an abrupt change in thermal expansion coefficient ( $\alpha_L$ ) from +15.5 ppm/°C to +11.4 ppm/°C. Assuming a linear relation between polarizability and temperature, an anomalous decrease in relative permittivity ( $\epsilon_r$ ) at  $T_{M-T}$  is predicted from the Clausius–Mosotti relation and Shannon's additive rule. Such an anomalous decrease in  $\epsilon_r$  at a phase transition has not previously been observed in ferroic and linear dielectrics and may aid in the design of novel microwave dielectric composites.

### Introduction

Microwave (MW) dielectric ceramic materials are widely used as dielectric resonators, filters, antenna substrates, and capacitors for wireless and mobile communication, radar and satellite positioning systems.<sup>1-4</sup> The large  $\epsilon_r$  (*real part of permittivity*) of MW dielectric ceramic helps reduce the dimensions of MW devices and low dielectric loss (high quality factor,  $Q$ ) enhances frequency selectivity.<sup>2-5</sup> Furthermore, their temperature stability with respect to resonant frequency (TCF) ensures that related devices work from -45 to 85 °C. 5th generation wireless systems (5G) have gradually come on-line in recent years and offer ultra-wideband, ultra-high speed, and ultra-low latency.<sup>6-8</sup> The frequency spectrum of 5G is generally divided into millimeter wave, mid-band and low-band.

Millimeter wave (above 24 GHz) is yet to be exploited but materials with  $\epsilon_r < 10$  are likely to be utilised.<sup>7-10</sup> Low-band refers to available frequency ranges at  $< 1$  GHz whereas mid-band will exploit 2-6 GHz interval and is the most widely deployed. To attain the required data transmission rates, massive MIMO (multiple input and multiple output) and Multi-User MIMO (MU-MIMO) antennas are employed that are composed of large numbers of interconnected devices.<sup>11-15</sup> Massive MIMO functions through mini base stations and exploits materials with  $\epsilon_r = 20$  such as  $\text{MgTiO}_3$ - $\text{CaTiO}_3$ ,  $(\text{Ca}_{1-x}\text{Sm}_x)(\text{Al}_{1-x}\text{Ti}_x)\text{O}_4$ , and  $\text{Li}_2\text{TiO}_3$  due to their high  $Q$  and low TCF.<sup>7, 16-19</sup>

Alongside the three materials mentioned above, fergusonite-structured  $\text{LnNbO}_4$  ( $\text{Ln}=\text{La}, \text{Sm}, \text{Nd}$  etc.) ceramics have attracted attention due to their high  $Q$  and  $\epsilon_r \sim 20$ .<sup>20-23</sup> Kim et al. first reported the microwave dielectric properties of  $\text{LaNbO}_4$  ceramic sintered at 1250 °C with  $\epsilon_r = 19.3$ , high  $Qf$  ( $Q \times$  resonant frequency,  $f$ )  $\sim 54,400\text{GHz}$  and  $\text{TCF} = +9$  ppm/°C.<sup>20</sup> Substitutions for La or Nb by isovalent ions plus the use of sintering aids further improve microwave dielectric properties.<sup>21-23</sup> with our previous work,<sup>21</sup> demonstrating that 10 mol. % substitution of  $\text{V}^{5+}$  for  $\text{Nb}^{5+}$  increases TCF from +9 ppm/°C to +110 ppm/°C.

TCF is approximately half the temperature coefficient of  $\epsilon_r$  ( $\tau_\epsilon$ ) according to:

$$\text{TCF} = -\frac{1}{2}\tau_\epsilon - \alpha_l \quad (1)$$

where  $\alpha_l$  is the linear thermal expansion coefficient (below +15 ppm/°C for ceramics). Hence, any abrupt change in TCF is normally attributed to a change in  $\tau_\epsilon$  usually caused by a structural phase transition. Phase transition which show an increase  $\epsilon_r$  are commonplace in ferroic materials as commonly observed for paraelectric to ferroelectric/antiferroelectric, ferroelectric to ferroelectric, octahedral tilt and paelastic to ferroelastic transformations.<sup>24-31</sup>

<sup>a</sup> Key Laboratory of Multifunctional Materials and Structures, Ministry of Education, School of Electronic Science and Engineering, Xi'an Jiaotong University, Xi'an 710049, Shaanxi, China

<sup>b</sup> Shaanxi Materials Analysis and Research Center, School of Materials Science and Engineering, Northwestern Polytechnical University, Xi'an, Shaanxi 710072, China

<sup>c</sup> Key Laboratory of Inorganic Functional Material and Device, Shanghai Institute of Ceramics Chinese Academy of Sciences, Shanghai 200050, China

<sup>d</sup> State Key Laboratory of Electrical Insulation and Power Equipment, Xi'an Jiaotong University, Xi'an 710049, Shaanxi, China

<sup>e</sup> Department of Materials Science and Engineering, University of Sheffield, S1 3JD, UK

<sup>f</sup> Micro-optoelectronic Systems Laboratories, Xi'an Technological University, Xi'an 710032, Shaanxi, China

<sup>g</sup> School of Electronics and Communication Engineering, Lovely Professional University, Jalandhar, Punjab, India

<sup>h</sup> National University of Science and Technology "MISIS", Leninskii Av., 4, Moscow, 4119049, Russia

<sup>i</sup> South Ural State University, Lenin Av., 76, Chelyabinsk, 454080, Russia

<sup>j</sup> Scientific and Practical Materials Research Center of the NAS of Belarus, P. Brovki Str., 19, Minsk, 220072, Belarus

\*Corresponding author E-mail address: zhoudi1220@gmail.com (Di Zhou) & i.m.reaney@sheffield.ac.uk (Ian M. Reaney).

Electronic Supplementary Information (ESI) available: [details of any supplementary information available should be included here]. See DOI: 10.1039/x0xx00000x

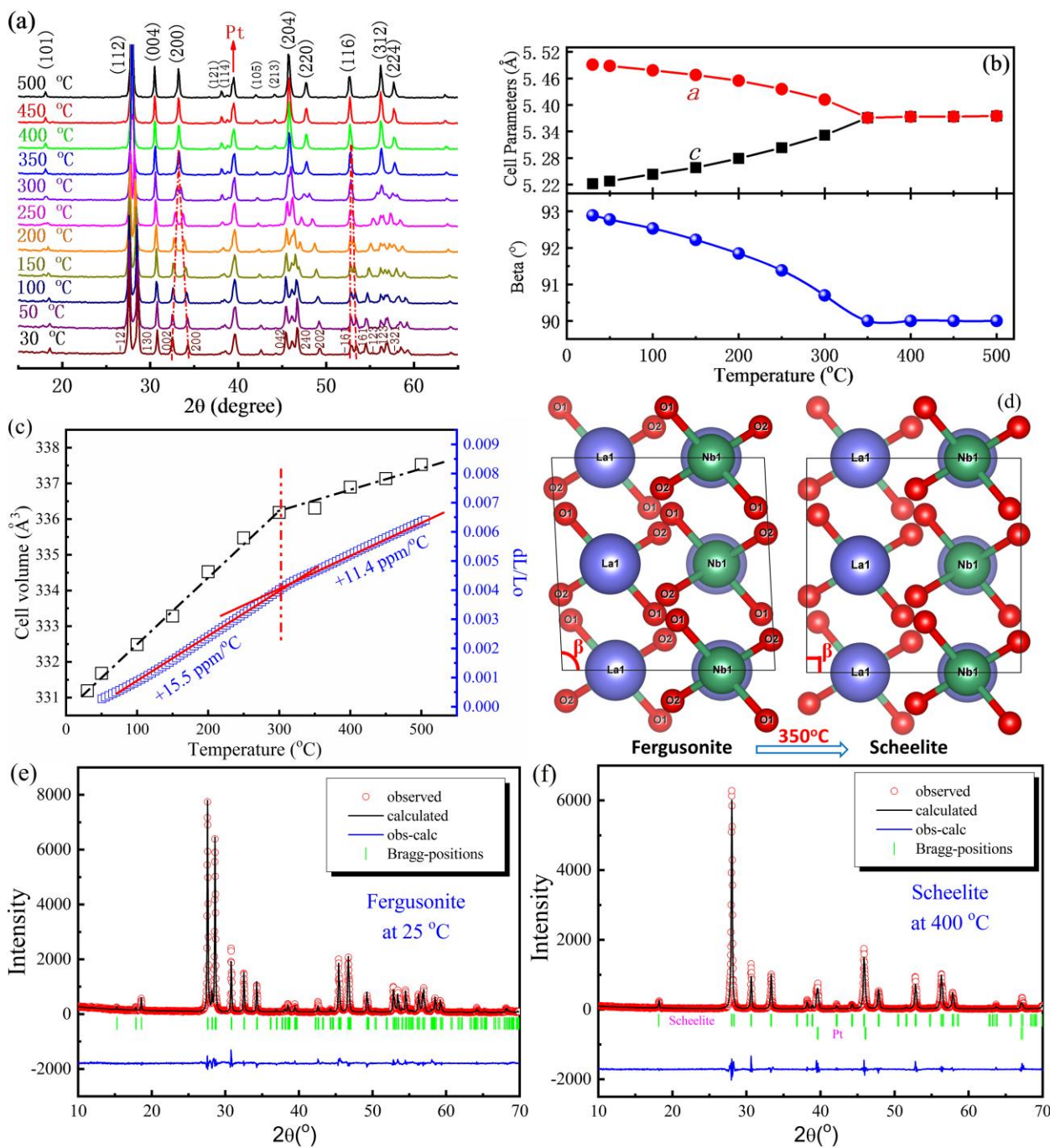


**Fig. 1.** (a) *In-situ* XRD patterns of the  $\text{La}(\text{Nb}_{0.9}\text{V}_{0.1})\text{O}_4$  ceramis from 30 ~ 500 °C. (b) cell parameters as a function of temperature. (c) cell volume and thermal expansion vs. temperature. (d) schematic of the change in crystal structure projected along the *b* axis. (e, f) experimental (circles) and calculated (line) XRD profiles for  $\text{La}(\text{Nb}_{0.9}\text{V}_{0.1})\text{O}_4$  at room temperature ( $R_p = 8.34\%$ ,  $R_{wp} = 11.5\%$ , and  $R_{exp} = 6.52\%$ ) and 400 °C ( $R_p = 10.9\%$ ,  $R_{wp} = 14.9\%$ , and  $R_{exp} = 9.84\%$ ). (The short vertical lines below the patterns mark Bragg reflections. The bottom continuous line is the difference between the observed and the calculated intensity).

All the above phase transitions occur through classical softening of a transverse optical mode, consistent with the Lyddane–Sach–Teller relation.<sup>32</sup> Since the maximum value of  $\epsilon_r$  occurs at the phase transition temperature (PTT/ $T_c$ ),  $\tau_\epsilon$  is largely positive below, but negative above the PTT, provided  $\epsilon_r$  is not too high. This principle is basis for the well-established relationship between tolerance factor and  $\tau_\epsilon$  described by Reaney et al.<sup>33</sup> in which octahedral tilting induces an increase in  $\epsilon_r$  at the PTT in Sr and Ba based complex perovskites. TCF follows the inverse trend. Similarly  $\text{BiVO}_4$  undergoes a second order ferroelastic phase transition from monoclinic ( $I2/a$ ) to

tetragonal scheelite ( $I4_1/a$ ) structure at 255 °C at which temperature a maximum value of  $\epsilon_r$  is observed.<sup>31, 34–38</sup> And in  $(\text{Li}_{0.5x}\text{Bi}_{1-0.5x})(\text{Mo}_x\text{V}_{1-x})\text{O}_4$  ( $0 \leq x \leq 0.25$ ) ceramics, peaks in  $\epsilon_r$  are observed at the PTT<sup>38, 39</sup> with corresponding changes in TCF.  $\text{LaNbO}_4$  also undergoes a ferroelastic phase transition from monoclinic fergusonite to tetragonal scheelite structure at ~480 °C.<sup>40–45</sup> From previous studies,<sup>21, 46</sup>  $\text{V}^{5+}$  substitutes for  $\text{Nb}^{5+}$  on the B site and lowers the PTT to room temperature, where the tetragonal scheelite structure is stabilized for  $x = 0.225$ . However, in  $\text{La}(\text{Nb},\text{V})\text{O}_4$  solid solutions, TCF decreases from a large positive (+100 ppm/°C) to large negative value (-

40 ppm/°C), the opposite trend to that which is typically observed at PTTs. This anomalous behaviour may be further elucidated by undertaking a detailed study of crystal structure as a function of temperature. In the present work therefore, we present *in-situ* XRD and Raman data in combination with thermal expansion measurement which are interpreted through Landau theory, Shannon's additive rule, and the Clausius–Mosotti relation. **Understanding of this behavior might lead to design of temperature stable composite materials in the future.**

## Materials and methods

**Material Synthesis.** Preparation of the  $\text{La}(\text{Nb}_{0.9}\text{V}_{0.1})\text{O}_4$  ceramic was described in detail in our previous work.<sup>21</sup>

**Material Characterization.** Room temperature XRD patterns were acquired using a Bruker D2 Phaser in the  $2\theta$  range 10–70°, with a step size of 0.02°. *In-situ* XRD patterns were collected using a Siemens D5000 diffractometer from 30 ~ 500 °C using Pt foil as holder for high temperature measurements. Results were analyzed by the Rietveld profile refinement method, using FULLPROF program. *In situ* Raman spectra were obtained with a Renishaw Raman microscope (model InVia) using a 532 nm solid state (100 mW) laser and a Linkam stage (model THMS600). Dielectric properties measurements were performed on sintered ceramics, diameter ~ 10 mm and thickness ~ 1 mm, coated with gold using a LCR (Agilent E4980A) and homemade heating system over from 25 to 680 °C at 10 kHz, 100 kHz, 250 kHz and 1 MHz with a heating rate 1 °C/min.

## Results and discussion

*In-situ* XRD patterns of the  $\text{La}(\text{Nb}_{0.9}\text{V}_{0.1})\text{O}_4$  ceramic in temperature range 30 ~ 500 °C and cell parameters as a function of temperature are shown in Fig. 1(a) and (b). At room temperature,  $\text{La}(\text{Nb}_{0.9}\text{V}_{0.1})\text{O}_4$  crystallized with a monoclinic fergusonite structure ( $I2/c$ ), with  $\text{V}^{5+}$  ions substituting for  $\text{Nb}^{5+}$ . As temperature increased, some characteristic peaks such as (121) and (130), (002) and (200), converged and merged into a single peak at ~350 °C, indicating a continuous structural transition from monoclinic fergusonite to tetragonal scheelite structure ( $I4_1/a$ ). Cell parameter  $a$  decreased with temperature while  $c$  increased and became equal to  $a$  at 350 °C, commensurate with a linear decrease in  $\beta$

**Table I.** Refined atomic fractional coordinates from XRD data for  $\text{La}(\text{Nb}_{0.9}\text{V}_{0.1})\text{O}_4$  sample at room temperature and the lattice parameters are  $a = 5.23654(7)$  Å,  $b = 11.6033(4)$  Å,  $c = 5.50762(4)$  Å,  $\beta = 92.894(4)^\circ$ . The space group is  $I2/c$  (15).

Atom	Site	Occ.	x	y	z
La	4e	0.5	0.25000	0.13539	0.00000
Nb	4e	0.45	0.25000	0.61890	0.00000
V	4e	0.05	0.25000	0.61890	0.00000
O1	8f	1.00	0.04142	0.71988	0.28695
O2	8f	1.00	1.02836	0.44614	0.19333

**Table II.** Refined atomic fractional coordinates from XRD data for the  $\text{La}(\text{Nb}_{0.9}\text{V}_{0.1})\text{O}_4$  sample at 400 °C and the lattice parameters are  $a = c = 5.3781(5)$  Å,  $b = 11.6783(7)$  Å. The space group is  $I4_1/a$  (88).

Atom	Site	Occ.	x	y	z
La	4b	0.25	0.00000	0.25000	0.62500
Nb	4a	0.20	0.00000	0.25000	0.12500
V	4a	0.05	0.00000	0.25000	0.12500
O	16f	1.000	0.15639	0.02148	0.20595

from 93° to 90°, Fig. 1(b). All data are therefore consistent with the premise that ~10 mol. %  $\text{V}^{5+}$  substitutes for  $\text{Nb}^{5+}$ , decreasing the distortion of the  $\text{BO}_4$  tetrahedra, lowering the ferroelastic phase transition temperature from 480 °C to 350 °C for undoped  $\text{LaNbO}_4$  and  $\text{La}(\text{Nb}_{0.9}\text{V}_{0.1})\text{O}_4$ , respectively.

Fig. 1(c) shows the cell volume and thermal expansion data of the  $\text{La}(\text{Nb}_{0.9}\text{V}_{0.1})\text{O}_4$  as a function of temperature. As temperature increased from 25 °C to 300 °C, the cell volume increased linearly from 331.19 Å<sup>3</sup> to 336.19 Å<sup>3</sup> corresponding to a gradient of +56 ppm/°C. The cell volume further increased to 337.53 Å<sup>3</sup> at 500 °C but the gradient decreased to +20 ppm/°C, suggesting a structural phase transition at ~350 °C. Thermal expansion coefficients also followed the same trend (Fig. 1(c)), abruptly changing from +15.5 ppm/°C to +11.4 ppm/°C at the proposed PTT. Fig. 1(d) is schematic illustrating the change in crystal structure along the  $b$  axis. In the fergusonite structure, B site ions (Nb,V) are located in the center of distorted tetrahedra with two B-O bonds lengths, resulting in different values of  $a$  and  $c$ , and a  $\beta$  angle >90 degrees. Above 350 °C, the B-O bond lengths in the tetrahedra become equal and the tetrahedral distortion disappears, coincident with  $\beta$  approaching 90 degrees. Cell refinements of fergusonite and scheelite structured  $\text{La}(\text{Nb}_{0.9}\text{V}_{0.1})\text{O}_4$  at room temperature and 400 °C are shown in Fig. 1(e) and (f), respectively. The refined lattice parameters of  $\text{La}(\text{Nb}_{0.9}\text{V}_{0.1})\text{O}_4$  at room temperature are  $a = 5.23654(7)$  Å,  $b = 11.6033(4)$  Å,  $c$

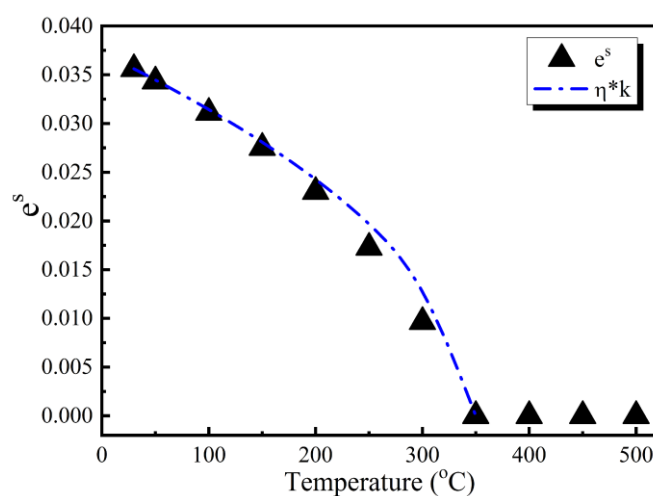


**Fig. 2.** Magnitude of the spontaneous strain and order parameter  $\eta$  of the  $\text{La}(\text{Nb}_{0.9}\text{V}_{0.1})\text{O}_4$  ceramic as a function of temperature.

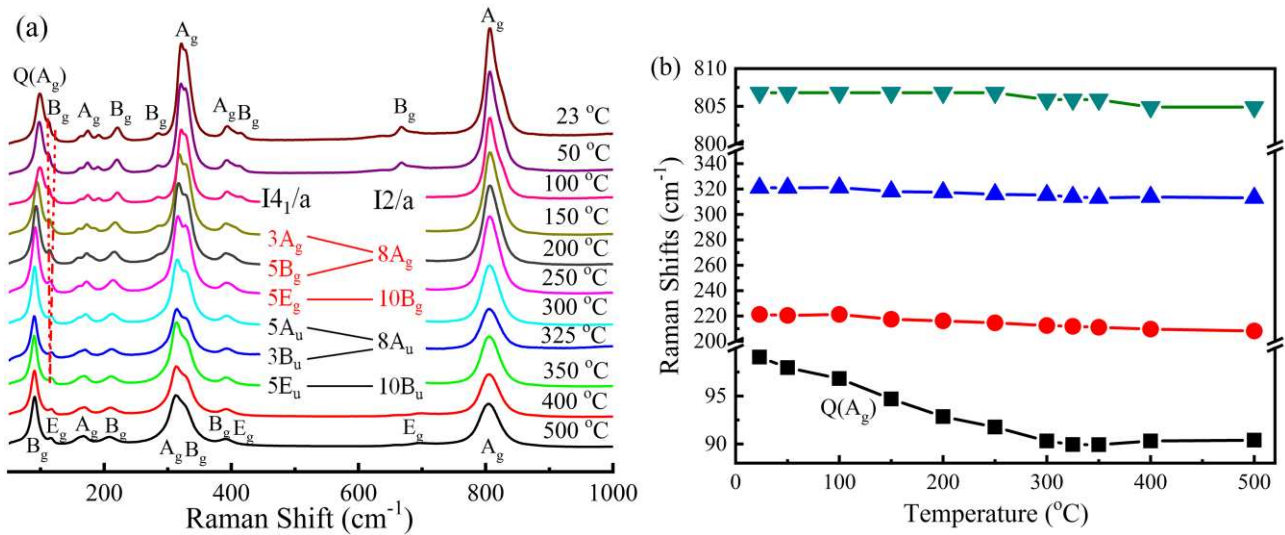


Fig. 3. (a) Raman shifts of  $\text{La}(\text{Nb}_{0.9}\text{V}_{0.1})\text{O}_4$  from 25–500 °C and (b) selected modes as a function of temperature.

$= 5.50762(4)$  Å, and  $\beta = 92.894(4)^\circ$  with space group  $I2/c$  (15) using data (ICSD # 81616) from Machida et al.<sup>47</sup> The refined lattice parameters of scheelite  $\text{La}(\text{Nb}_{0.9}\text{V}_{0.1})\text{O}_4$  at 400 °C are  $a = c = 5.3781(5)$  Å,  $b = 11.6783(7)$  Å with a space group  $I4_1/a$  (88) from (ICSD # 37139) reported by David.<sup>48</sup> Atomic fractional coordinates and structure details are listed in Table I and II. Clear domains could be observed from the room temperature TEM images of  $\text{La}(\text{Nb}_{0.9}\text{V}_{0.1})\text{O}_4$  ceramic as shown in Fig. S1 in Supporting Information and agree well with XRD data.

The ferroelastic phase transition from monoclinic fergusonite to tetragonal scheelite is associated with an increase in point group symmetry from  $2/m$  to  $4/m$  and results in merging of two crystal orientation states ( $S_1$  and  $S_2$ ) above PTT. Hence, second rank strain tensors can be employed to describe these two orientation states caused by the relative ‘monoclinic’ displacements to paraelastic scheelite phase:<sup>49, 50</sup>

$$e_{ij}(S_1) = \begin{pmatrix} e_{11} & e_{12} & 0 \\ e_{21} & e_{22} & 0 \\ 0 & 0 & e_{33} \end{pmatrix}, \quad (2)$$

$$e_{ij}(S_2) = R e_{ij}(S_1) R^T, \quad (3)$$

where  $R$  and  $R^T$  are the  $90^\circ$  rotation matrix and its transposition, respectively. As reported by Schlenker et al.,<sup>51</sup> strain tensor components can be calculated from the cell parameters:

$$e_{11} = \frac{c_m \times \sin(\beta_m)}{a_t} - 1,$$

$$e_{22} = \frac{a_m}{a_t} - 1,$$

$$e_{33} = \frac{b_m}{c_t} - 1,$$

$$e_{12} = e_{21} = \frac{1}{2} \times \frac{c_m \times \cos(\beta_m)}{a_t},$$

where  $a_m$ ,  $b_m$ ,  $c_m$  and  $\beta_m$  are cell parameters of monoclinic phase, and  $c_t$  and  $c_b$  are the extrapolated tetragonal phase cell parameters. As described by Aizu,<sup>49</sup> ferroelasticity can be quantified using the spontaneous strain tensors and the two possible orientation states of  $\text{La}(\text{Nb}_{0.9}\text{V}_{0.1})\text{O}_4$  are presented:

$$e_{ij}^s(S_1) = \begin{pmatrix} -\mu & \nu & 0 \\ \nu & \mu & 0 \\ 0 & 0 & 0 \end{pmatrix}, \quad (4)$$

$$e_{ij}^s(S_2) = \begin{pmatrix} \mu & -\nu & 0 \\ -\nu & -\mu & 0 \\ 0 & 0 & 0 \end{pmatrix}, \quad (5)$$

where  $\mu = \frac{1}{2}(e_{22} - e_{11})$  is the longitudinal strain and  $\nu = e_{12}$  is the shear strain. It follows that the magnitude of the spontaneous strain is:

$$e^s = \sqrt{\mu^2 + \nu^2}, \quad (6)$$

The spontaneous strain of the  $\text{La}(\text{Nb}_{0.9}\text{V}_{0.1})\text{O}_4$  ceramic is  $\sim 3.55\%$  at room temperature, approximately half that of undoped  $\text{LaNbO}_4$  ceramic (6.79%).

According to Landau theory,<sup>52</sup> the order parameter,  $\eta$  (equ. 7) may be used to describe the deviation from the paraelastic phase:

$$\eta = \left( \frac{T_c - T}{T} \right)^{1/2}, \quad (7)$$

where  $T_c$  is PTT, (350 °C) and  $T$  is temperature. The magnitude of the spontaneous strain of  $\text{La}(\text{Nb}_{0.9}\text{V}_{0.1})\text{O}_4$  is proportional to  $\eta$  according to:

$$e^s = \eta \times k, \quad (8)$$

where  $k$  is a constant (0.03725). The  $\eta \times k$  and  $e^s$  values as a function of temperature were plotted in Fig. 2. From room to the phase transition temperature, agreement between  $\eta \times k$  and  $e^s$  is obtained, confirming that the transition is second order.

Group theory predicts that there are 18 Raman active modes for monoclinic fergusonite structure ( $I2/a$ ) and irreducible representation of the modes are:<sup>53, 54</sup>

$$\Gamma = 8A_g + 10B_g + 8A_u + 10B_u, \quad (9)$$

where  $A_g$  and  $B_g$  are Raman active while  $A_u$  and  $B_u$  are IR active. For the tetragonal scheelite structure ( $I4_1/a$ ), the irreducible representation according to the group theory is given by:<sup>55, 56</sup>

$$\Gamma = 3A_g + 5B_g + 5E_g + 5A_u + 3B_u + 5E_u, \quad (10)$$

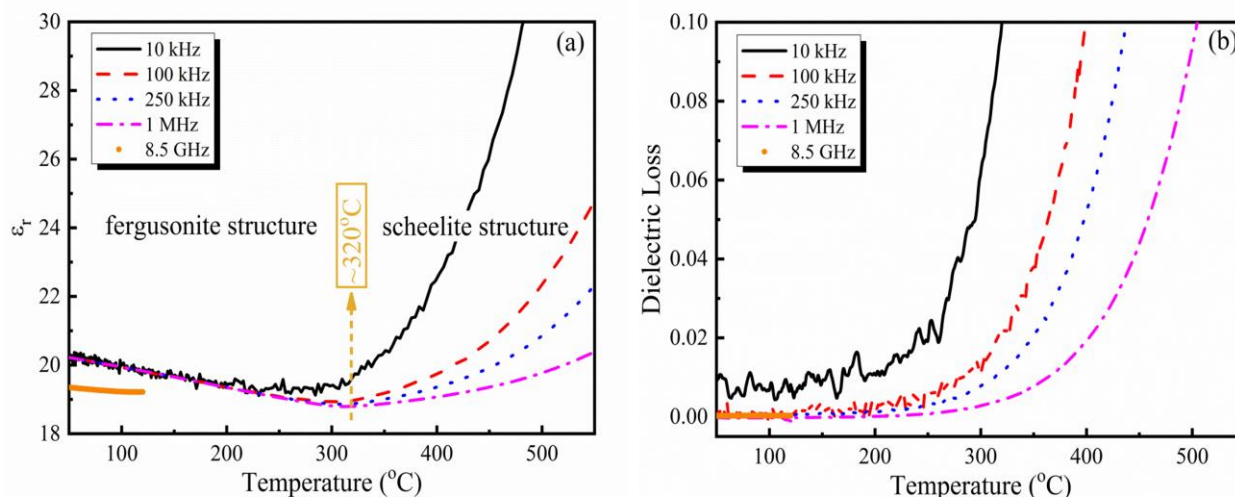


Fig. 4. (a, b)  $\epsilon_r$  and dielectric loss of the  $\text{La}(\text{Nb}_{0.9}\text{V}_{0.1})\text{O}_4$  ceramic as a function of temperature at different frequencies (10 kHz, 100 kHz, 250 kHz, 1 MHz and 8.5 GHz).

where all the  $A_g$ ,  $B_g$  and  $E_g$  are Raman active and all the  $A_u$  and  $E_u$  are IR active. The correlation of the representations is at  $\Gamma$  points of the  $I2/a$  and  $I4_1/a$  space groups. The phase transition in  $\text{La}(\text{Nb}_{0.9}\text{V}_{0.1})\text{O}_4$  may be described as a proper ferroelastic with strain as the primary order parameter, dominated by a soft acoustic phonon (marked Q in Fig. 3a). Based on Landau theory,<sup>54</sup>  $\omega_Q$  below PTT ( $T_C$ ) is given as follows:

$$\omega_Q \approx \omega_{Q0} + \frac{\delta c'_0}{2\omega_{Q0}T_0}(T_C - T), \quad (11)$$

where,  $\omega_{Q0}$  is the frequency at  $T_C$ ,  $\delta c'_0$  is a spontaneous shear strain parameter, and  $T_0$  is the temperature at which ferroelastic phase becomes unstable.  $\omega_Q$  decreases linearly with temperature in the ferroelastic but remains constant in the paraelastic phase, which agrees with experimental results, Fig. 3b, where  $\omega_{Q0}$  is  $\sim 90 \text{ cm}^{-1}$ . For  $\text{BiVO}_4$ , the ferroelastic  $\rightarrow$  paraelastic phase transition is driven by a temperature dependent  $B_g$  optic mode coupled to the acoustic

soft mode as described by Pinczuk et al.<sup>37, 57</sup> In contrast to  $\text{BiVO}_4$ , no soft optical mode has been observed from room temperature to 500  $^{\circ}\text{C}$ , which defines the phase transition in  $\text{LaNbO}_4$  is purely ferroelastic with strain as the sole order parameter.<sup>54, 58</sup> Hence, the Lyddane-Sachs-Teller (LST) relation is not followed.

$\epsilon_r$  and dielectric loss of the  $\text{La}(\text{Nb}_{0.9}\text{V}_{0.1})\text{O}_4$  ceramic as a function of temperature at different frequencies (10 kHz, 100 kHz, 250 kHz, 1 MHz and 8.5 GHz) are shown in Fig. 4. Different from the situations in  $\text{BiVO}_4$  ferroelastic ceramics and other ferroics as shown in Fig. 5b, an anomalous  $\epsilon_r$  minimum value was observed at 10 kHz, 100 kHz, 250 kHz, and 1 MHz. Due to the limit of microwave dielectric measurement, we didn't obtain the wide temperature microwave  $\epsilon_r$  spectrum but the present data shows an apparent decrease of permittivity vs. temperature, which gives a large positive TCF value. Compared with  $\epsilon_r$ , there is no abnormality observed from dielectric loss

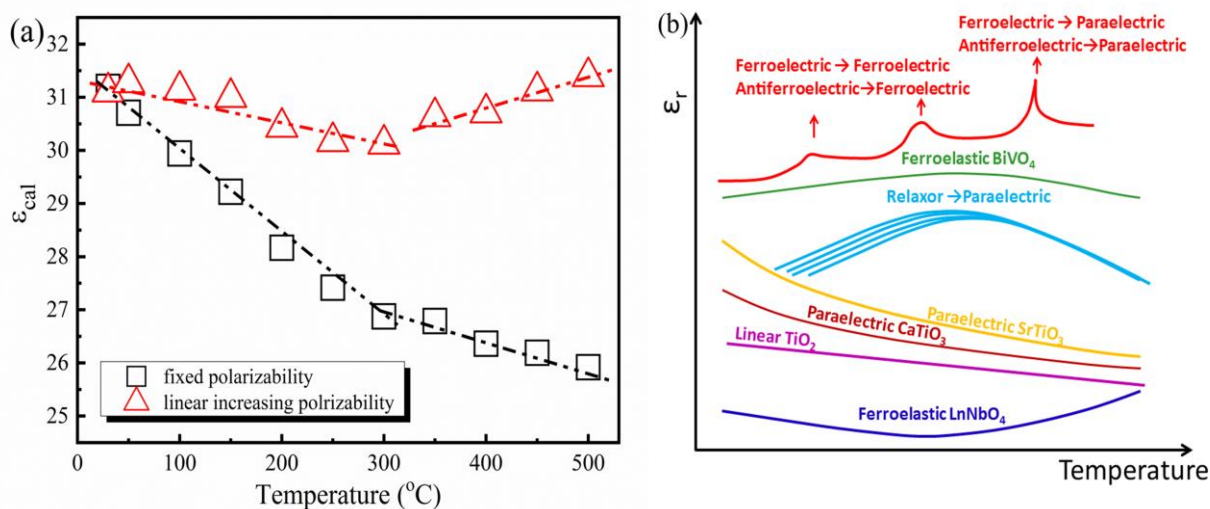


Fig. 5. (a) Calculated dielectric constant of  $\text{La}(\text{Nb}_{0.9}\text{V}_{0.1})\text{O}_4$  ceramic on assumptions of fixed and linear increasing polarizabilities and (b) schematic of  $\epsilon_r$  of typical electro-ceramics vs. temperature.

as shown Fig. 4(b). In the microwave region, polarizability is the sum of both ionic and electronic components. Shannon<sup>59</sup> suggested that molecular polarizability ( $\alpha$ ) of complex substances may be estimated by summing  $\alpha$  of the constituent ions which for  $\text{La}(\text{Nb}_{0.9}\text{V}_{0.1})\text{O}_4$  is:

$$\alpha_{\text{La}(\text{Nb}_{0.9}\text{V}_{0.1})\text{O}_4} = \alpha_{\text{La}^{3+}} + 0.9 \times \alpha_{\text{Nb}^{5+}} + 0.1 \times \alpha_{\text{V}^{5+}} + 4\alpha_{\text{O}^{2-}} = 17.98 \text{ \AA}^3, \quad (12)$$

where the ionic polarizabilities of  $\text{La}^{3+}$ ,  $\text{Nb}^{5+}$ ,  $\text{V}^{5+}$  and  $\text{O}^{2-}$  are 6.07  $\text{\AA}^3$ , 3.97  $\text{\AA}^3$ , 2.92  $\text{\AA}^3$  and 2.01  $\text{\AA}^3$ , respectively.<sup>59</sup> Considering the Clausius–Mosotti (C-M) relation,<sup>60</sup>

$$\epsilon_{\text{cal}} = \frac{3V + 8\pi\alpha}{3V - 4\pi\alpha} \approx 31.1, \quad (13)$$

where  $V$  is the cell volume ( $331.19/4 = 82.8 \text{ \AA}^3$ ). The calculated  $\epsilon_r$  is 31.1, much larger than the measured value ( $\sim 20$ ) at room temperature. As reported by Tsunekawa et al.,<sup>40, 44, 53</sup>  $\text{BO}_4$  tetrahedra are distorted in the fergusonite structure. The distorted tetrahedra have reduced B–O bond lengths, dampen B–O lattice vibrations and thereby decrease polarizability. Furthermore, macroscopic polarizability also includes additional terms related to the crystal structure and local anisotropy. As reported by Feteira et al.,<sup>61</sup> polarizabilities of lanthanides (Ln) were derived from rare-earth aluminates system and it became evident that Ln (e.g.  $\text{La}^{3+} = 4.68 \text{ \AA}^3$ ) have lower values than reported by Shannon.<sup>59</sup>

The C-M relation indicates that  $\epsilon_r$  of a specific compound is determined both by cell volume and molecular polarizability. For  $\text{La}(\text{Nb}_{0.9}\text{V}_{0.1})\text{O}_4$ , as temperature increased, cell volume increased linearly below and above 350 °C but with different gradients. Based on the assumption that molecular polarizability does not change with temperature,  $\epsilon_r$ , calculated using equation (13), is plotted in Fig. 5a which reveals a linear decrease below and above 350 °C but at different gradients. There is therefore, an anomaly at 350 °C but not a minimum value of  $\epsilon_r$ . However, if we assume that molecular polarizability increases with temperature and follows a simple linearly relation:

$$\alpha_{\text{La}(\text{Nb}_{0.9}\text{V}_{0.1})\text{O}_4} = \alpha_0 + (T - T_R) \times k, \quad (14)$$

where  $\alpha_0$  is the room temperature molecular polarizability, 17.975  $\text{\AA}^3$ ,  $T_R$  is room temperature and  $k$  (0.00075) is a temperature dependent constant, the combined effect of cell volume and molecular polarizability vs.  $T$  gives a minimum value of  $\epsilon_r$  at PTT as shown in Fig. 5a. Although this is a rough calculation, it gives a clear explanation for the dielectric minimum of  $\text{La}(\text{Nb}_{0.9}\text{V}_{0.1})\text{O}_4$  ceramic at the PTT, at which point a decrease in thermal expansion coefficient occurs. In Fig. 5b, we summarize the possible curves of  $\epsilon_r$  vs.  $T$  for a ferroelectric, relaxor, antiferroelectric, ferroelastic, paraelectric and linear dielectric material. The purely ferroelastic character and the sudden decrease in thermal expansion coefficient for  $\text{La}(\text{Nb}_{0.9}\text{V}_{0.1})\text{O}_4$  are anomalous compared with conventional ferroics and dielectrics.

## Conclusions

The  $\text{La}(\text{Nb}_{0.9}\text{V}_{0.1})\text{O}_4$  ceramic was determined by *in-situ* XRD analysis to undergo a ferroelastic phase transition from

monoclinic fergusonite to tetragonal scheelite structure at  $\sim 350$  °C. Raman analysis identified strain as the sole order parameter with a value of 3.55% at room temperature, almost half that of pure  $\text{LaNbO}_4$  ceramic. At the PTT, there was an abrupt change of thermal expansion coefficient from +15.5 ppm/°C to +11.4 ppm/°C, related to the anomalous change in cell volume. Assuming a linear increase in polarizability, the minimum value  $\epsilon_r$  at the PTT for  $\text{La}(\text{Nb}_{0.9}\text{V}_{0.1})\text{O}_4$  was predicted from the Clausius–Mosotti relation and Shannon's additive rule. Compared with ferroelectrics, relaxors, antiferroelectrics, ferroelastics, paraelectrics and linear dielectrics, the behaviour of  $\epsilon_r$  in  $\text{La}(\text{Nb}_{0.9}\text{V}_{0.1})\text{O}_4$  vs temperature is anomalous and may have novel applications in temperature stable composite ceramics.

## Conflicts of interest

There are no conflicts to declare.

## Acknowledgements

This work was supported by the National Key Research and Development Program of China (Grant 2017YFB0406301), Sustainability and Substitution of Functional Materials and Devices EPSRC (EP/L017s563/1), the National Natural Science Foundation of China (51972260, 52072295), the State Key Laboratory of Electrical Insulation and Power Equipment (Grant EIPE19210), the Fundamental Research Funds for the Central University, and the 111 Project of China (B14040).

## References

- I. M. Reaney and D. Iddles, Microwave dielectric ceramics for resonators and filters in mobile phone networks, *J. Am. Ceram. Soc.*, 2006, **89**, 2063–2072.
- T. Fujii, A. Ando and Y. Sakabe, Characterization of dielectric properties of oxide materials in frequency range from GHz to THz, *J. Eur. Ceram. Soc.*, 2006, **26**, 1857–1860.
- H. Ohsato, T. Tsunooka, A. Kan, Y. Ohishi, Y. Miyauchi, Y. Tohdo, T. Okawa, K. Kakimoto and H. Ogawa, Microwave-millimeterwave dielectric materials, *Key Eng. Mater.*, 2004, **269**, 195–198.
- M. T. Sebastian and H. Jantunen, Low loss dielectric materials for LTCC applications: a review, *Int. Mater. Rev.*, 2008, **53**, 57–90.
- M. T. Sebastian, R. Uvic and H. Jantunen, Low-loss dielectric ceramic materials and their properties, *Int. Mater. Rev.*, 2015, **60**, 392–412.
- D. Zhou, L. X. Pang, D. W. Wang, C. Li, B. B. Jin and I. M. Reaney, High permittivity and low loss microwave dielectrics suitable for 5G resonators and low temperature co-fired ceramic architecture, *J. Mater. Chem. C*, 2017, **5**, 10094–10098.
- H. H. Guo, D. Zhou, C. Du, P. J. Wang, W. F. Liu, L. X. Pang, Q. P. Wang, J. Z. Su, C. Singh and S. Trukhanov, Temperature stable  $\text{Li}_2\text{Ti}_{0.75}(\text{Mg}_{1/3}\text{Nb}_{2/3})_{0.25}\text{O}_3$ -based microwave dielectric ceramics with low sintering temperature and ultra-low dielectric loss for dielectric resonator antenna applications, *J. Mater. Chem. C*, 2020, **8**, 4690–4700.
- H. H. Guo, D. Zhou, W. F. Liu, L. X. Pang, D. W. Wang, J. Z. Su and Z. M. Qi, Microwave dielectric properties of

- temperature-stable zircon-type (Bi, Ce)VO<sub>4</sub> solid solution ceramics, *J. Am. Ceram. Soc.*, 2020, **103**, 423-431.
- 9 C. H. Lee, N. D. Orloff, T. Birol, Y. Zhu, V. Goian, E. Rocas, R. Haislmaier, E. Vlahos, J. A. Mundy, L. F. Kourkoutis, Y. Nie, M. D. Biegalski, J. Zhang, M. Bernhagen, N. A. Benedek, Y. Kim, J. D. Brock, R. Uecker, X. X. Xi, V. Gopalan, D. Nuzhnyy, S. Kamba, D. A. Muller, I. Takeuchi, J. C. Booth, C. J. Fennie and D. G. Schlom, Exploiting dimensionality and defect mitigation to create tunable microwave dielectrics, *Nature*, 2013, **502**, 532-536.
  - 10 N. M. Dawley, E. J. Marks, A. M. Hagerstrom, G. H. Olsen, M. E. Holtz, V. Goian, C. Kadlec, J. Zhang, X. Lu, J. A. Drisko, R. Uecker, S. Ganschow, C. J. Long, J. C. Booth, S. Kamba, C. J. Fennie, D. A. Muller, N. D. Orloff and D. G. Schlom, Targeted chemical pressure yields tuneable millimetre-wave dielectric, *Nat. Mater.*, 2020, **19**, 176-181.
  - 11 O. Elijah, C. Y. Leow, T. A. Rahman, S. Nunoo and S. Z. Iliya, A comprehensive survey of pilot contamination in Massive MIMO—5G system, *IEEE Commun. Surv. Tut.*, 2016, **18**, 905-923.
  - 12 K. Xiao, L. Gong and M. Kadoch, Opportunistic multicast NOMA with security concerns in a 5G Massive MIMO system, *IEEE Commun. Mag.*, 2018, **56**, 91-95.
  - 13 M. B. Krishna and J. Lloret Mauri, *Advances in mobile computing and communications : perspectives and emerging trends in 5G networks*, CRC Press, Boca Raton, 2016.
  - 14 Y. H. Jung, J. Lee, Y. Qiu, N. Cho, S. J. Cho, H. Zhang, S. Lee, T. J. Kim, S. Gong and Z. Ma, Stretchable twisted-pair transmission lines for microwave frequency wearable electronics, *Adv. Funct. Mater.*, 2016, **26**, 4635-4642.
  - 15 I. Khan, M. Zafar, M. Jan, J. Lloret, M. Basher and D. Singh, Spectral and energy efficient low-overhead uplink and downlink channel estimation for 5G Massive MIMO systems, *Entropy*, 2018, **20**, 92.
  - 16 H. Li, B. Tang, X. Li, Z. Qing, Y. Li, H. Yang, Q. Wang and S. Zhang, The structure and properties of 0.95MgTiO<sub>3</sub>–0.05CaTiO<sub>3</sub> ceramics doped with Co<sub>2</sub>O<sub>3</sub>, *J. Mater. Sci.*, 2014, **49**, 5850-5855.
  - 17 X. C. Fan and X. M. Chen, Effects of Ca/Ti cosubstitution upon microwave dielectric characteristics of CaSmAlO<sub>4</sub> ceramics, *J. Am. Ceram. Soc.*, 2009, **92**, 433-438.
  - 18 L. X. Pang and D. Zhou, Microwave dielectric properties of low - firing Li<sub>2</sub>MO<sub>3</sub> (M=Ti, Zr, Sn) Ceramics with B<sub>2</sub>O<sub>3</sub> - CuO addition, *J. Am. Ceram. Soc.*, 2010, **93**, 3614-3617.
  - 19 H. H. Guo, D. Zhou, L. X. Pang and J. Z. Su, Influence of (Mg<sub>1/3</sub>Nb<sub>2/3</sub>) complex substitutions on crystal structures and microwave dielectric properties of Li<sub>2</sub>TiO<sub>3</sub> ceramics with extreme low loss, *J. Materiomics*, 2018, **4**, 368-382.
  - 20 D. W. Kim, D. K. Kwon, S. H. Yoon and K. S. Hong, Microwave dielectric properties of rare-earth ortho-niobates with ferroelasticity, *J. Am. Ceram. Soc.*, 2006, **89**, 3861-3864.
  - 21 D. Guo, D. Zhou, W. B. Li, L. X. Pang, Y. Z. Dai and Z. M. Qi, Phase evolution, crystal structure, and microwave dielectric properties of water-insoluble (1-x)LaNbO<sub>4</sub>-xLaVO<sub>4</sub> (0 ≤ x ≤ 0.9) ceramics, *Inorg. Chem.*, 2017, **56**, 9321-9329.
  - 22 H. W. Lee, J. H. Park, S. Nahm, D. W. Kim and J. G. Park, Low-temperature sintering of temperature-stable LaNbO<sub>4</sub> microwave dielectric ceramics, *Mater. Res. Bull.*, 2010, **45**, 21-24.
  - 23 F. Vullum, F. Nitsche, S. M. Selbach and T. Grande, Solid solubility and phase transitions in the system LaNb<sub>1-x</sub>Ta<sub>x</sub>O<sub>4</sub>, *J. Solid State Chem.*, 2008, **181**, 2580-2585.
  - 24 A. R. V. Hippel, Ferroelectricity, domain structure, and phase transitions of barium titanate, *Rev. Mod. Phys.*, 1950, **22**, 221-237.
  - 25 M. Acosta, N. Novak, V. Rojas, S. Patel and J. Rödel, BaTiO<sub>3</sub>-based piezoelectrics: Fundamentals, current status, and perspectives, *Appl. Phys. Rev.*, 2017, **4**, 041305.
  - 26 B. Noheda, N. Cereceda, T. Iglesias, G. Lifante and L. W. Yong, Composition dependence of the ferroelectric-paraelectric transition in the mixed system PbZr<sub>1-x</sub>Ti<sub>x</sub>O<sub>3</sub>, *Phys. Rev. B*, 1995, **51**, 16388-16391.
  - 27 A. K. Tagantsev, K. Vaideswaran, S. B. Vakhruhev, A. V. Filimonov, R. G. Burkovsky, A. Shaganov, D. Andronikova, A. I. Rudskoy, A. Q. Baron, H. Uchiyama, D. Chernyshov, A. Bosak, Z. Ujma, K. Roleder, A. Majchrowski, J. H. Ko and N. Setter, The origin of antiferroelectricity in PbZrO<sub>3</sub>, *Nat. Commun.*, 2013, **4**, 2229.
  - 28 G. Shirane and R. Pepinsky, Phase transitions in antiferroelectric PbHfO<sub>3</sub>, *Phys. Rev.*, 1953, **91**, 812-815.
  - 29 D. L. Corker, A. M. Glazer, W. Kaminsky, R. W. Whatmore, J. Dec and K. Roleder, Investigation into the crystal structure of the perovskite lead hafnate, PbHfO<sub>3</sub>, *Acta Cryst.*, 1998, **54**, 18-28.
  - 30 P. D. Dernier and J. P. Remeika, Synthesis and symmetry transformation in the perovskite compounds PbHfO<sub>3</sub> and CdHfO<sub>3</sub>, *Mater. Res. Bull.*, 1975, **10**, 187-192.
  - 31 R. M. Hazen and J. W. E. Mariathasan, Bismuth vanadate: a high-pressure, high-temperature crystallographic study of the ferroelastic-paraelectric transition, *Science*, 1982, **216**, 991-993.
  - 32 R. H. Lyddane, R. G. Sachs and E. Teller, On the polar vibrations of alkali halides, *Phys. Rev.*, 1941, **59**, 673-676.
  - 33 I. M. Reaney, E. L. Colla and N. Setter, Dielectric and structural characteristics of Ba-based and Sr-based complex perovskites as a function of tolerance factor, *Jpn. J. Appl. Phys.*, 1994, **33**, 3984-3990.
  - 34 J. D. Bierlein and A. W. Sleight, Ferroelasticity in BiVO<sub>4</sub>, *Solid State Commun.*, 1975, **16**, 69-70.
  - 35 W. I. F. David, A. M. Glazer and A. W. Hewat, The structure and ferroelastic phase transition of BiVO<sub>4</sub>, *Phase Transit.*, 1979, **1**, 155-169.
  - 36 A. W. Sleight, H. Y. Chen, A. Ferretti and D. E. Cox, Crystal growth and structure of BiVO<sub>4</sub>, *Mater. Res. Bull.*, 1979, **14**, 1571-1581.
  - 37 A. Pinczuk, B. Welber and F. H. Dacol, Mechanism of the ferroelastic transition of BiVO<sub>4</sub>, *Solid State Commun.*, 1979, **29**, 515-518.
  - 38 D. Zhou, W. G. Qu, C. A. Randall, L. X. Pang, H. Wang, X. G. Wu, J. Guo, G. Q. Zhang, L. Shui, Q. P. Wang, H. C. Liu and X. Yao, Ferroelastic phase transition compositional dependence for solid-solution [(Li<sub>0.5</sub>Bi<sub>0.5</sub>)<sub>x</sub>Bi<sub>1-x</sub>][Mo<sub>x</sub>V<sub>1-x</sub>]O<sub>4</sub> scheelite-structured microwave dielectric ceramics, *Acta Mater.*, 2011, **59**, 1502-1509.
  - 39 D. Zhou, C. A. Randall, H. Wang, L. X. Pang and X. Yao, Ultra-low firing high-k scheelite structures based on [(Li<sub>0.5</sub>Bi<sub>0.5</sub>)<sub>x</sub>Bi<sub>1-x</sub>][Mo<sub>x</sub>V<sub>1-x</sub>]O<sub>4</sub> microwave dielectric ceramics, *J. Am. Ceram. Soc.*, 2010, **93**, 2147-2150.
  - 40 S. Tsunekawa and H. Takei, Domain switching behaviour of ferroelastic LaNbO<sub>4</sub> and NdNbO<sub>4</sub>, *J. Phys. Soc. Jpn.*, 1976, **40**, 1523-1524.
  - 41 L. H. Brixner, J. F. Whitney, F. C. Zumsteg and G. A. Jones, Ferroelasticity in the LnNbO<sub>4</sub>-type rare earth niobates, *Mater. Res. Bull.*, 1977, **12**, 17-24.
  - 42 V. S. STUBIČAN, High-temperature transitions in rare-earth niobates and tantalates, *J. Am. Ceram. Soc.*, 1964, **47**, 55-58.
  - 43 K. A. Gingerich and H. E. Bair, Relation between ionic radii and transformation temperature in rare earth niobates, *Adv. X-Ray Anal.*, 1964, **7**, 22-30.
  - 44 H. Takei and S. Tsunekawa, Growth and properties of LaNbO<sub>4</sub> and NdNbO<sub>4</sub> single crystals, *J. Cryst. Growth*, 1977, **38**, 55-60.
  - 45 W. I. F. David, *Structural phase transitions in ferroic ABO<sub>4</sub> crystals*, Ph.D. thesis, University of Oxford, 1981.
  - 46 S. Wachowski, A. Mielewczyk-Gryn and M. Gazda, Effect of isovalent substitution on microstructure and phase transition

- of  $\text{LaNb}_{1-x}\text{M}_x\text{O}_4$  (M=Sb, V or Ta;  $x=0.05\text{--}0.3$ ), *J. Solid State Chem.*, 2014, **219**, 201-209.
- 47 M. Machida, J. Kido, T. Kobayashi, S. Fukui, N. Koyano and Y. Suemune, X-ray investigation on the crystal and domain structures of  $\text{LaNbO}_4$ , *Annu. Rep. Res. React. Inst. Kyoto Univ.*, 1995, **28**, 25-32.
- 48 W. I. F. David, The high-temperature paraelastic structure of  $\text{LaNbO}_4$ , *Mater. Res. Bull.*, 1983, **18**, 749-756.
- 49 Aizu and K itsiro, Possible species of ferromagnetic, ferroelectric, and ferroelastic crystals, *Phys. Rev. B*, 1970, **2**, 754-772.
- 50 P. Satin, R. W. Hughes, D. R. Lowry, Z. D. Apostolov and W. M. Kriven, High-temperature properties and ferroelastic phase transitions in rare-earth niobates ( $\text{LnNbO}_4$ ), *J. Am. Ceram. Soc.*, 2014, **97**, 3307-3319.
- 51 J. L. Schlenker, G. V. Gibbs and M. B. Boisen, Strain-tensor components expressed in terms of lattice parameters, *Acta Crystallogr. A*, 1978, **34**, 52-54.
- 52 L. D. Landau, On the theory of phase transitions, *Zh. Eksp. Teor. Fiz.*, 1937, **7**, 19-32.
- 53 S. Tsunekawa, H. Takei and M. Ishigame, Study on the room temperature phase of  $\text{LaNbO}_4$  crystals, *Mater. Res. Bull.*, 1977, **12**, 1087-1094.
- 54 M. Wada, Y. Nakayama, A. Sawada, S. Tsunekawa and Y. Ishibashi, Raman scattering and fluorescence spectra of  $\text{LaNbO}_4$ , *J. Phys. Soc. Jpn.*, 1979, **47**, 1575-1580.
- 55 M. Nicol and J. F. Durana, Vibrational Raman spectra of  $\text{CaMoO}_4$  and  $\text{CaWO}_4$  at high pressures, *J. Chem. Phys.*, 1971, **54**, 1436-1440.
- 56 D. Christofilos, G. A. Kourouklis and S. Ves, A high pressure Raman study of calcium molybdate, *J. Phys. Chem. Solids*, 1995, **56**, 1125-1129.
- 57 A. Pinczuk, G. Burns and F. H. Dacol, Soft optical phonon in ferroelastic  $\text{BiVO}_4$ , *Solid State Commun.*, 1977, **24**, 163-165.
- 58 B. Y. Gu, H. Z. Cummins, S. L. Qiu and M. Copic, Acoustic soft modes and the ferroelastic phase transition in  $\text{BiVO}_4$  and  $\text{LaNbO}_4$ , *Ferroelectrics*, 1983, **52**, 45-57.
- 59 R. D. Shannon, Dielectric polarizabilities of ions in oxides and fluorides, *J. Appl. Phys.*, 1993, **73**, 348-366.
- 60 P. V. Rysselberghe, Remarks concerning the Clausius-Mossotti law, *J. Phys. Chem.*, 1932, **36**, 1152-1155.
- 61 A. Feteira, D. C. Sinclair and M. T. Lanagan, Structural and electrical characterization of  $\text{CeAlO}_3$  ceramics, *J. Appl. Phys.*, 2007, **101**, 064110.